

Deformation of dark solitons in inhomogeneous Bose-Einstein condensates

N.G. Parker, N.P. Proukakis, M. Leadbeater, and C.S. Adams

Department of Physics, University of Durham, South Road, Durham DH1 3LE, United Kingdom

E-mail: n.g.parker@durham.ac.uk

Abstract. A dark soliton becomes unstable when it is incident on a background density gradient, and the induced instability results in the emission of sound. Detailed quantitative studies of sound emission are performed for various potentials, such as steps, linear ramps and gaussian traps. The amount of sound emission is found to be a significant fraction of the soliton energy for typical potentials. Continuous emission of sound is found to lead to an apparent deformation of the soliton profile. The power emitted by the soliton is shown to be parametrised by the square of the displacement of the centre of mass of the soliton from its density minimum, thus highlighting the significance of the inhomogeneity-induced soliton deformation.

PACS numbers: 03.75.Lm, 42.65.Tg

1. Introduction

The intrinsic similarities between the Gross-Pitaevskii equation describing the zero-temperature mean-field dynamics of Bose-Einstein condensates (BEC) and the cubic nonlinear Schrodinger equation (NLSE) of nonlinear optical systems implies the existence of common fundamental phenomena, independent of the origin of the nonlinearity. For example, experiments on BEC's have recently led to the observation of four-wave mixing of matter waves [1], and both bright [2, 3] and dark [4, 5, 6] matter wave solitons. Solitons are, strictly speaking, shape-preserving one-dimensional excitations supported in nonlinear media, where the effect of dispersion is balanced by the interatomic interactions. Three-dimensional analogs of solitons, so-called solitary waves, do exist, but are more prone to instabilities than their one-dimensional counterparts [7]. In the context of nonlinear optics, solitons propagate in the effectively one-dimensional (1D) medium of homogeneous optical fibers. Bright solitons find applications in optical communications [8], whereas potential applications of the less exploited dark solitons include the formation of zero cross-talk optical junctions [9]. In the case of atomic BEC's, 1D geometries have been recently engineered by suitable combination of optical and magnetic traps [10, 11], and also on microchips [12, 13, 14].

The one-dimensional Gross-Pitaevskii Equation (GPE) describing trapped atomic BEC's is given by

$$i\hbar \frac{\partial \psi}{\partial t} = -\frac{\hbar^2}{2m} \frac{\partial^2}{\partial x^2} \psi + V_{\text{ext}} \psi + g|\psi|^2 \psi - \mu \psi. \quad (1)$$

Here ψ corresponds to the macroscopic order parameter of the system, V_{ext} is the necessary external confining potential and m is the atomic mass. The effective 1D interaction coefficient g arises by assuming an axially symmetric elongated three-dimensional system and integrating out the transverse ground state wavefunctions. This leads to $g = 2\hbar^2 a / (ml_{\perp}^2)$, where l_{\perp} is the transverse harmonic oscillator length and a is the s -wave scattering length. The validity of a purely 1D description of a quasi-1D system has been considered elsewhere [15, 16, 17, 18, 19]. Also, $\mu = gn$ corresponds to the chemical potential of the system, with the condensate density denoted by n . In the absence of an external potential (i.e. $V_{\text{ext}} = 0$), Eq. (1) becomes exactly integrable and supports dark solitary wave solutions [20]. On a uniform background density n , a dark soliton with speed v and position $(x - vt)$ has the analytical form,

$$\psi(x, t) = \sqrt{n} e^{-i(\mu/\hbar)t} \left(\beta \tanh \left[\beta \frac{(x - vt)}{\xi} \right] + i \left(\frac{v}{c} \right) \right). \quad (2)$$

Here $\beta = \sqrt{1 - (v/c)^2}$, and the soliton speed v is intimately dependent on both the soliton depth n_d (with respect to the background density), and the total phase slip S across the centre. It is given by $v = \sqrt{n - n_d} = c \cos(S/2)$, the limiting value being set by the Bogoliubov speed of sound $c = \sqrt{\mu/m}$. A stationary soliton features a π phase slip and a maximal depth $n_d = n$, while a soliton with speed c is effectively indistinguishable from the background fluid. The healing length $\xi = \hbar/\sqrt{\mu m}$ characterises the width of the soliton.

In the case of nonlinear optics, an equation analogous to the homogeneous version of Eq. (1) arises for nonlinear media with $\chi^{(3)}$ susceptibilities, for which ψ would correspond to the electric field amplitude. Imperfections in $\chi^{(3)}$ crystals are unavoidable, and lead, in general, to perturbations of the susceptibility. This essentially introduces modifications to Eq. (1), which arise, for example, due to

transiting, saturable or competing nonlinearities [21]. Any deviation from the homogeneous form of Eq. (1) breaks its integrability and induces instability in the soliton. As a result, the soliton emits radiation and can subsequently decay. The rate of energy loss of the soliton due to modified nonlinearities has been shown to be proportional to the local acceleration squared [22]. In the case of atomic BEC's, the integrability of Eq. (1) is broken due to the external confining potential $V_{\text{ext}} \neq 0$ within which experiments are performed. In addition to the effects of transverse degrees of freedom [17, 18, 19, 23, 24, 25], the integrability of the system is broken by the applied longitudinal potential which induces the soliton to radiate sound [18, 19, 26, 27].

If the change in the background potential is weak, then, to first order, the soliton dynamics are similar to those of an effective particle of constant (negative) mass [28, 29, 30]. In general, however, the sound emission leads to a change in the soliton effective mass, and hence a change in its subsequent trajectory [18, 19, 26, 27, 31]. To monitor this change, one can apply a perturbative approach [32, 33], which will be valid as long as the potential does not vary significantly over the size of the soliton. However, if the density changes over a prolonged region, leading to continuous sound emission, then the total emitted energy can be a significant fraction of the initial soliton energy, and, consequently, the *net* change in the soliton dynamics can be significant. In previous work we have quantified the amount of sound emission and the stability of dark solitons in quasi-1D BEC's, suggesting how this can be both controlled and measured experimentally in realistic traps [19]. In this paper we discuss in more detail the dynamics of solitons incident on various inhomogeneities, with the aim to highlight the importance of the apparent *deformation* that a soliton undergoes when incident on a potential gradient. This deformation is a direct consequence of the sound energy trapped within the soliton region, as the soliton propagates on the background density gradient. The rate of emission of sound energy by the soliton will be shown to be proportional to the square of the deformation parameter, identified as the displacement of the observed soliton centre of mass (i.e. including local sound energy within the soliton region) from the soliton (density) minimum. We will further show that the acceleration of a soliton through the fluid is directly proportional to the soliton deformation parameter, thus simultaneously confirming the validity of an acceleration squared sound emission law for various potentials.

This paper is structured as follows: Sec. 2 discusses the dynamics of dark solitons incident on potential steps of variable length and height. This analysis reveals the dissipative nature of the soliton motion and, in particular, highlights the significant proportion of the soliton energy that can be radiated as sound. In this section, we further quantify the sound emission as a function of the step geometry. The scattering of a soliton by a barrier of finite width contains a number of subtle features which are discussed in Sec. 2.2. The appearance of soliton deformation becomes more apparent when considering the case of a constant background density gradient, which can be provided by a linear ramp (Sec. 3). To discuss the deformation in more detail, and to give results which are directly relevant to atomic BEC experiments, Sec. 4 focuses on a soliton oscillating in a double gaussian trap. This enables us to probe a large range of background density gradients, and thus show that the rate of sound emission can be parametrised in terms of the square of the induced soliton deformation. Finally, Sec. 5 contains some concluding remarks.

2. Dark Soliton incident on a potential step

Consider initially a dark soliton on a homogeneous background incident on a potential step, as shown schematically in Fig. 1(a). For an effectively infinitely long step of constant (finite) height, this situation corresponds to soliton propagation between two homogeneous regions of different background density. This is similar to bright soliton propagation at the interface between two nonlinear dielectric media of different refractive indices, arising in the context of nonlinear optics. This has been discussed within the effective (or equivalent) particle theory, which treats the bright soliton as a particle of fixed effective mass moving in an effective potential created by the interface between the two media [34]. Such an approach ignores radiative effects, which have however been included, to lowest order, in a perturbative treatment [35, 36].

A soliton incident on a step of *finite* length can represent the presence of impurities, or optically-engineered barriers. Huang *et al.* [37] have predicted that a dark soliton interacting with a steplike potential emits radiation, and in the case where the step is downward, the soliton is prone to fission into multiple solitons. Frantzeskakis *et al* [38] recently considered the interaction of a dark soliton with an impurity (without explicitly discussing sound generation), whereas a subsequent paper [39] addressed the possibility to trap solitons in time-dependent potentials. Soliton-impurity interactions have also been discussed in [40], where the expected sound emission could not be observed due to computational constraints.

To study such systems in more detail, we consider a potential of the form,

$$V(x) = \begin{cases} 0 & \text{for } x \leq 0, x \geq L \\ V_0 & \text{for } 0 < x < L \end{cases} \quad (3)$$

where V_0 is the height and L the length of the step. In our subsequent numerical analysis, we employ dimensionless units, with distance and velocity measured in terms of the healing length ξ and the speed of sound c respectively. In addition the asymptotic number density n_0 is rescaled to unity. The initial state is taken as the product $\psi(x, 0) = \sqrt{n(x)}\psi_s(x, 0)$, with the soliton centred on a locally flat background density. Here $n(x)$ is the time-independent background density obtained by imaginary time propagation of the GPE, and $\psi_s(x, 0)$ corresponds to the homogeneous analytic soliton solution of Eq. (2).

2.1. Infinitely long step

Consider initially the case of a very long ($L \rightarrow \infty$) positive ($V_0 > 0$) step, as illustrated in Fig. 1(a). This can be thought of as a transition between two different homogeneous regions. To understand the ensuing soliton dynamics it is important to note that the time-independent background density consists of the usual Thomas-Fermi solution, $n(x) = n_0(x) - V(x)$, plus a tanh-like smoothing of the boundary region resulting from fluid healing. A positive step therefore induces a lower background density in the second region (II). The different regimes of the dynamics of a dark soliton incident on such a boundary are summarized in Fig. 1. In particular, Fig. 1(b) shows characteristic paths of a dark soliton with fixed initial speed incident on steps of different heights V_0 (cases (i)-(iv), in order of increasing V_0). Although this figure is based on a particular *initial* soliton speed, the qualitative behaviour analysed here is characteristic of the general crossover between the two regions.

For low steps heights (Fig. 1b(i)) the soliton, initially in region (I), is able to pass over the boundary, and emits a burst of counter-propagating sound pulses. This

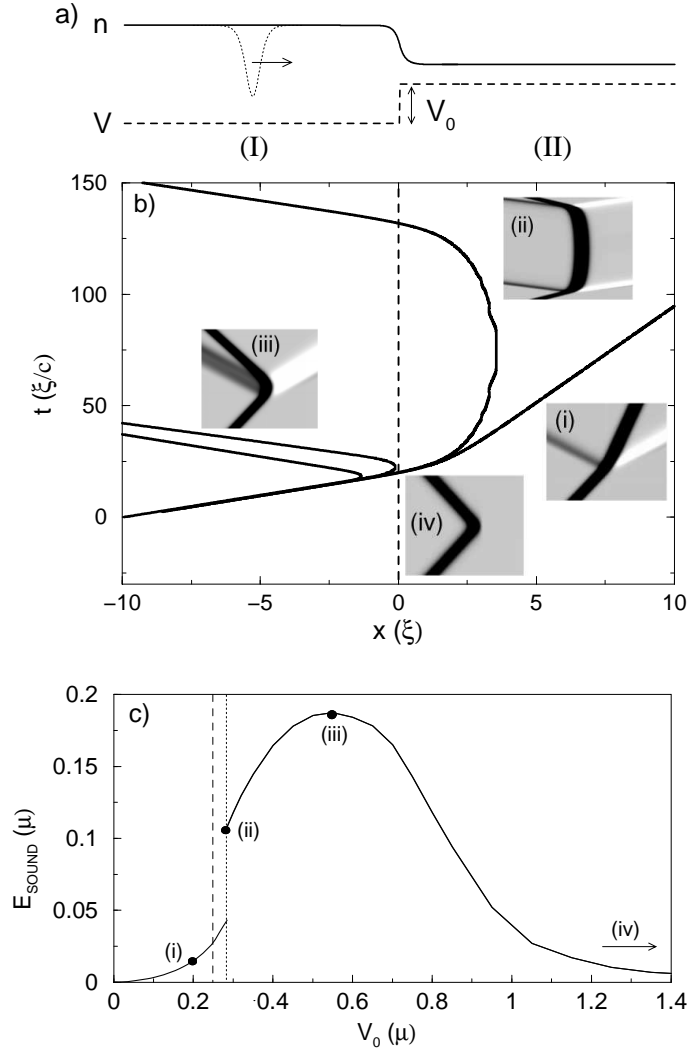


Figure 1. a) Dark soliton incident on an infinitely long step of height V_0 (dashed line). The corresponding background fluid density is shown schematically by a solid line, while the dotted line indicates the dark soliton propagating on the background fluid. b) Path of a soliton, initially in region (I) with speed $0.5c$, incident on a potential step of infinite length (region (II)). We identify four regimes, in order of increasing step height: (i) transmission over the step ($V_0 = 0.2\mu$), (ii) reflective quasi-trapping at the boundary ($V_0 = 0.267\mu$), (iii) reflection with maximum sound emission ($V_0 = V_0^m = 0.55\mu$), and (iv) elastic collision ($V_0 \gg \mu$), where $\mu = \hbar c/\xi$. Corresponding space-time carpet plots for each case highlight excitations on top of the background density, with counter-propagating sound pulses clearly visible for cases (i)-(iii). c) Total emitted sound energy as a function of step height V_0 , with the cases (i)-(iv) from Fig. 1(b) highlighted. The point of reflection (represented by the dotted line) occurs for larger step heights than predicted for an effective constant mass particle (dashed line), as a result of sound emission. The discontinuity arises from the fact that, during transmission a single burst of sound is emitted, while for reflection, there are two bursts, when the soliton passes both on and off the step.

sound serves to remove excess phase from the soliton as it is forced to adapt to the new ambient density. The radiation travels at the speed of sound and disperses over time. Once the soliton has fully traversed the barrier and entered the second homogeneous region, it propagates with reduced (but constant) speed, due to the lower ambient density and hence reduced speed of sound. The emission of sound tends to slightly increase the speed of the soliton, but this is only a minor effect compared to the decrease in the soliton speed due to the lower background density. Increasing the step height results in the soliton becoming “refracted” to a greater extent. This ultimately leads to reflection, when the kinetic energy becomes insufficient to ascend the potential (Fig. 1b(ii)), with the amount of ‘penetration’ into the second region decreasing with increasing step height (Fig. 1b(iii)). Assuming, as a first approximation, that both energy and depth of the soliton remain conserved, the threshold for transmission would be $V_0 = v^2$, i.e., when the soliton with depth $(1 - v^2)$ can *just* transmit into the far region with density $(1 - V_0)$. However, the process of sound emission tends to reduce the soliton depth and increase its speed. This leads to the appearance of a regime in which the soliton can be transmitted even though the corresponding constant mass particle would be reflected (see next section). In this case sound is still radiated by the soliton as it ascends and descends the bump. Finally, in the limit of collision with a hard wall ($V_0 \rightarrow \infty$, i.e. soliton incident on a region of zero density), the soliton reflects elastically without breaking up or decaying, irrespective of the incident speed (Fig. 1b(iv)). Note that the soliton reverses direction before its centre of mass actually reaches the boundary. This is analogous to the head-on collision of two solitons whereby momentum can be exchanged without the centres having crossed, and leads to the idea that the soliton undergoes a virtual collision with its corresponding mirror image [37]. The fact that the macroscopic wavefunction tends to zero at the wall implies a singularity in the macroscopic phase, allowing the soliton to reset its phase such that incoming and outgoing speeds are the same, which corresponds to elastic reflection.

The analogy to refraction of light at an optical interface leads to the question of whether there is a critical step height where the soliton becomes permanently trapped at the boundary. We find a critical regime where the soliton becomes ‘quasi-trapped’ at the boundary (Fig. 1b(ii)), but that, within our resolution, the ultimate fate of the soliton is to either transmit or reflect [38]. However, the soliton can indeed become *almost* stationary at the boundary for a relatively long time, during which it makes a significant passage into the classically forbidden region. For example, for a soliton with initial speed $0.5c$ and a carefully selected step height $V_0 = 0.2666\mu$, we have observed quasi-trapping for times of $\sim 1500(\xi/c)$ and the density minimum extending $\sim 7\xi$ into the far region, before returning to the first region. Two separate bursts of sound radiation are observed as the soliton passes on and off the step. A closer inspection also reveals small-scale sound emission in the intervening time.

In the regime $V_0 < 0$, i.e., when the soliton travels to a higher density region, we find similar results. Here the soliton is always transmitted, sound is emitted, and the soliton speed increases due to the increased speed of sound. We fail to observe the disintegration of the incident soliton into multiple solitons predicted by Huang *et al* [37]. In fact, we find that the soliton structure is unbreakable by the potential step, and conclude that the main decay channel is through sound emission.

The soliton energy can be calculated by integrating the energy functional,

$$\varepsilon(\psi) = \frac{\hbar^2}{2m} |\nabla\psi|^2 + V_{\text{ext}} |\psi|^2 + \frac{g}{2} |\psi|^4, \quad (4)$$

across the soliton region (say $x_s \pm 5\xi$) [41] and subtracting the corresponding contribution of the background fluid. This procedure cannot discriminate between soliton and sound energy present in the interval, and this will be shown to be intimately linked to the apparent soliton deformation. The total emitted sound energy is shown in Fig. 1(c) as a function of step height, with the four characteristic cases of Fig. 1(b) highlighted. Its form is a result of the interplay between the magnitude of the density gradient experienced by the soliton and the reduced density in the second region, which tends to suppress sound transmission. For low step heights, the soliton has sufficient energy to transmit into region (II), emitting a single burst of sound energy as it passes onto the step. Subsequently the soliton remains in region (II), and the energy loss is determined by comparing the energy within the ‘soliton region’ in regions (II) and the initial soliton energy. As the step height increases, so do the depth and gradient of the background density perturbation, leading to an initial increase in sound emission. At $V_0 \approx 0.28\mu$ (dotted line in Fig. 1(c)), the soliton no longer has enough energy to be transmitted, and thus eventually returns to region (I), after spending a finite time on, or near, the interface between the two regions. In this case, the final soliton energy is measured once the soliton has fully returned to region (I). Hence, in this regime of quasi-trapping/reflection, the soliton emits two bursts of sound: one as it ascends the boundary, and another as it passes back off the boundary. This leads to a sudden increase (roughly doubling) of the emitted sound energy, as evident in Fig. 1(c). The total sound emission initially increases further beyond this point, until the density gradient *experienced by the soliton* saturates. However the depth of the density inhomogeneity continues to increase, thus suppressing sound propagation into the second region and leading to a net reduction in the sound emission. It is important to note that the total energy released can be considerable: for the case (iii) in Fig. 1, approximately 22% of the soliton energy is converted into sound.

2.2. Step of finite length

To perform a more detailed study of the dissipative soliton dynamics, we now consider a dark soliton incident on a step of finite length L , as illustrated in Fig. 2(a). The important parameter determining whether a soliton is transmitted at a barrier is the ‘effective’ density seen by the moving soliton due to fluid healing in the vicinity of the step (solid line in Fig. 2(a)). For sufficiently narrow steps, fluid healing prohibits the density from reaching the Thomas-Fermi value, $n(x) = n_0(x) - V(x)$. The minimum density n_{\min} to which the fluid actually heals can be used to define an effective potential of height $V_{\text{eff}} = (1 - n_{\min})$. Fig. 2(b) maps the effective potential for steps of variable length and height. This suggests that for small enough step widths, the soliton may see an effective step height much lower than the actual potential, thus enabling the soliton to tunnel through barriers for which a classical particle would undergo elastic reflection. Assuming no dissipation, then, to leading order, the requirement for transmission would be that $V_{\text{eff}} < v^2$. Thus, for a soliton with incident speed $v = 0.5c$, the $V_{\text{eff}} = 0.25\mu$ contour of Fig. 2(b) represents, to first order, the critical region between transmission and reflection. The *actual* crossover between reflection and transmission is shown by the solid line in Fig. 2(b), which clearly shows the deviation resulting from the inhomogeneity-induced emission of sound from the soliton.

Fig. 2(c) shows the corresponding total sound emitted from the soliton, the magnitude of which is intimately related to the above-mentioned effective potential.

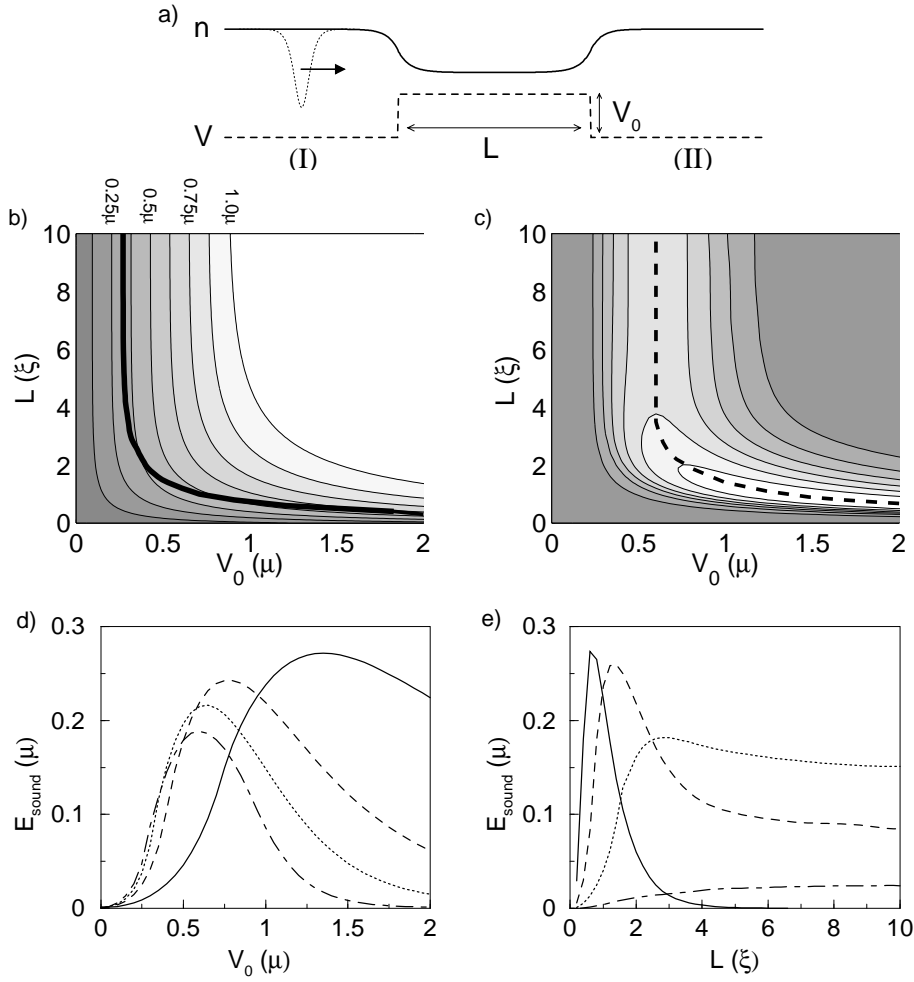


Figure 2. a) Soliton incident on a finite potential step (dashed line) of length L and height V_0 . The step causes a reduction in the background fluid density (solid line), through which the soliton (dotted line) propagates. b) Effective potential imposed by the step as a function of length and height, with each contour representing an increment of 0.125μ . An effective potential of unity implies a pinning of the density to zero. Although higher effective potentials exist, we do not show them here as, throughout this limit, the sound emission is essentially prohibited. Note that for effective potentials slightly greater than unity, the density is weakly pinned to zero and sound of positive amplitude can just propagate through. The solid line indicates the transition between reflection/transmission for a soliton with initial speed $v = 0.5c$ (the non-dissipative prediction would be the $V_{\text{eff}} = 0.25\mu$ contour). c) Total sound emitted from a dark soliton with initial speed $v = 0.5c$ and energy $E_s = 0.866\mu$ incident on a step of height V_0 and length L . The emitted energy ranges from zero (darkest region) to maximum value in equal contour steps. Maximum sound emission occurs along the dashed line $V_0 = V_0^m(L)$. d) Cross-sections of c) for constant step lengths of $L = \xi$ (solid line), 2ξ (dashed line), 5ξ (dotted line) and 10ξ (dot-dashed line). e) Cross-sections of c) for constant step heights of $V_0 = 0.25\mu$ (dot-dashed line), 0.5μ (dotted line), μ (dashed line) and 2μ (solid line).

Maximum sound emission occurs in the region of reflective quasi-trapping where the soliton is subject to its greatest acceleration/deformation. The line of maximum sound emission, defined by $V_0 = V_0^m(L)$, is highlighted by the dashed line in Fig. 2(c). Note that $V_0^m(L)$ decreases with increasing length, and essentially saturates to the value of $V_0^m(L) \approx 0.6\mu$ for $L \geq 5\xi$. The maximum sound energy released in Fig. 2(c) is approximately 0.27μ , which corresponds to 32% of the initial soliton energy. The sound emission tails off in the opposite limiting cases of $V_0, LEq.(4)_0 \rightarrow 0$ and $V_0, L_0 \rightarrow \infty$. To visualize the behaviour more clearly, Fig. 2(d)-(e) plot, respectively, the total emitted sound energy (i.e. both forward and backward sound pulses) as a function of step height V_0 (for various fixed step widths L) and as a function of L (for various fixed V_0).

Fig. 2(d) shows that, for fixed L , the total emitted sound increases abruptly with increasing step height, reaches a maximum at the point of reflective quasi-trapping, and decreases more slowly as $V_0 \rightarrow \infty$, similar to the behaviour encountered in the last section. Note that the variation of the emitted energy with step height is smooth and does not feature the discontinuity apparent in Fig. 1(c) for an infinitely long step. This can be understood as follows: for a soliton transmitting over an *infinitely* long step, a single burst of energy is emitted before the soliton reaches its steady state on the step, whereas a soliton which is ultimately reflected interacts *twice* with the boundary, thus emitting two sound pulses. In the case of a *finite* length step, this distinction does not arise. For transmission, the soliton must ascend and descend the step before reaching its steady state on the far side of the step (where its final energy is to be computed). This clearly involves two bursts of energy being radiated. However, the case of reflection also features two bursts, occurring when the soliton ascends and descends the first boundary. Since the background fluid is symmetric around the centre of the step (as regions (I) and (II) have the same potentials), the net amount of sound emission in the two limiting cases of soliton marginally transmitting, or just reflecting, will be the same, and hence the discontinuity will be absent here.

To understand in more detail the features of Fig. 2(d), it is instructive to consider the effective potential experienced by the soliton in each of the three limiting cases, namely (i) transmission ($V_0 \ll V_0^m(L)$), (ii) reflection with maximum energy emission (occurring at $V = V_0^m(L)$), and (iii) reflection with sound emission ($V_0 \gg V_0^m(L)$), but still far from the $V_0 \rightarrow \infty$ limit. These are shown in figures ((a)-(c)), respectively. Different lines in each of these figures correspond to different step widths ($L = \xi, 2\xi, 5\xi$ and 10ξ). (Note that the step heights in Fig. 3(b) differ from line to line.) For a constant step width L , the density depression becomes more pronounced with increasing step height (this can be visualized, e.g. by looking at the change of the solid line corresponding to $L = \xi$ from (a)-(c)). Fig. 3(a) shows the case of soliton transmission over the entire step ($V_0 = 0.25\mu$). Note that the particular soliton under consideration, with initial speed $0.5c$ and depth $0.75n_0$, can probe, to first order, densities down to $0.75n_0$ before being forced to change direction. Such a soliton can therefore just transmit in this case. In this limit of transmission, maximum sound emission occurs when the soliton traverses the steepest background density gradient for the longest time. Clearly this occurs for maximum step width $L = 10\xi$ (dot-dashed line). Fig. 3(c) shows the other extreme case, when the soliton is completely reflected, as a result of experiencing a very high potential ($V_0 = 2\mu$). In the case of a sufficiently long step, e.g. $L = 10\xi$ (dot-dashed line) in Fig. 3(c), the fluid heals fully to the Thomas-Fermi limit, thus reaching zero density. The soliton effectively sees a hard wall and becomes reflected without any sound emission (see corresponding

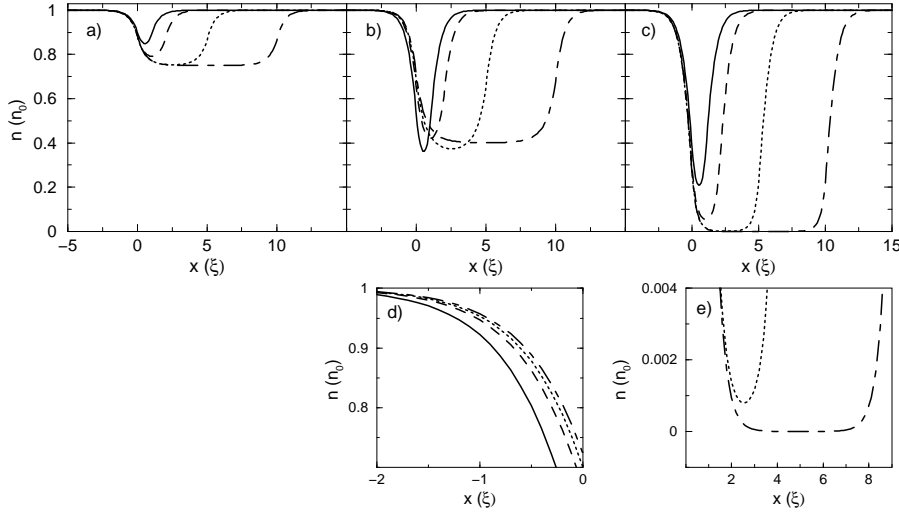


Figure 3. Background density profiles due to fluid healing in the region of the step. Each sub-figure plots the cases of $L = \xi$ (solid line), 2ξ (dashed line), 5ξ (dotted line) and 10ξ (dot-dashed line) as in Fig. 2(d) for different potential heights V_0 : (a) Transmitted soliton at $V_0 = 0.25\mu$, (b) Reflected soliton at $V_0 = V_0^m(L)$ corresponding to maximum sound emission for each L , i.e. at $V_0^m(\xi) = 1.36\mu$ (solid line), $V_0^m(2\xi) = 0.77\mu$ (dashed line), $V_0^m(5\xi) = 0.64\mu$ (dotted line) and $V_0^m(10\xi) = 0.60\mu$ (dot-dashed line). (c) Reflected soliton at $V_0 = 2\mu$. (d) Enlarged image of the background density inhomogeneity experienced by the soliton in (b), in the region $-2 < x < 0$ for $L = \xi$, 2ξ , 5ξ , and 10ξ . In this region, the density gradient is clearly maximized for the narrowest step ($L = \xi$, solid line), (e) Enlarged image of (c) showing the effective minimum density in the cases $L = 5\xi$ (dotted) and $L = 10\xi$ (dashed). This shows that for a width $L = 5\xi$ (dotted line), the density does not quite heal to zero, allowing a small amount of sound transmission through the barrier. Note that such density profiles can also be obtained by matching analytically known solutions of the Gross-Pitaevskii equation in finite and semi-infinite intervals (see, e.g. [42, 43]).

dot-dashed line in Fig. 2(d) at $V_0 = 2\mu$). However, as the step width is decreased, the reflected soliton can emit increasing amounts of sound energy. This is because the finite density at the step now enables *sound propagation* into the second region, despite the fact that the *soliton* is reflected. Note that, despite appearing to do so, the dotted line of Fig. 3(c) does *not* reach zero density (see Fig. 3(e) showing enlarged version of Fig. 3(c) near $n = 0$). This explains why there is some (albeit limited) sound emission for $L = 5\xi$ (dotted line) at $V_0 = 2\mu$ in Fig. 2(d).

Although this accounts for the qualitative features of the lines in Fig. 2(d), it still does not explain why the *maximum* emitted energy for narrow steps (e.g. solid line in Fig. 2(d) at $V_0 = V_0^m(L = \xi) \approx 1.4\mu$) is larger than the *maximum* emitted energy for longer steps (e.g. dashed line of same figure). To explain this, we must examine the background density profile for each of the lengths considered (i.e. $L = \xi$, 2ξ , 5ξ and 10ξ) at the step height which corresponds to maximum sound emission. As evident from Figs. 2(c)-(d), this critical barrier height $V_0 = V_0^m$ depends also on the step width (i.e. $V_0 = V_0^m(L)$). Therefore, to interpret the increase in the maximum emitted energy for narrower steps, we must compare the effective background densities

for different widths L at their corresponding heights $V_0 = V_0^m(L)$. This is illustrated in Fig. 3(b). To first approximation, in all these cases (i.e. all L), the soliton probes the step region down to a density of approximately $(1 - v^2)$ (corresponding to $0.75n_0$ for the soliton under consideration), before being reflected. Consequently, the soliton is approximately limited to the $x < 0$ region. Therefore, the key parameter controlling the amount of sound radiation is the *gradient* of the background density probed by the soliton (which clearly depends on the step width). To see this gradient clearer, Fig. 3(d) plots an enlarged version of the effective potentials of Fig. 3(b) in the region $-2\xi < x < 0$. Hence, at the point of maximum emission for each L , it is actually the *narrower* step (solid line) which has the *steepest* gradient. As a result, the *maximum* sound emission occurs for narrower steps. We have hence accounted for the entire behaviour of the emitted sound energy as a function of step height.

From the above analysis, one can also understand the features of Fig. 2(e) showing the dependence of emitted energy on step width. For small V_0 (e.g. $V_0 = 0.25\mu$, dot-dashed line) the soliton is transmitted, releasing maximum sound for longest steps, with the amount saturating for $L \rightarrow \infty$. Increasing V_0 (e.g. $V_0 = 0.5\mu$, dotted line) leads to larger density gradients and hence more sound emission as $L \rightarrow \infty$. The peak emitted energy at $L \approx 2.7\xi$ is due to a maximum time spent on the step in the regime of reflective quasi-trapping. Increasing V_0 further leads to the gradual suppression of sound transmission and hence a reduced total sound emission in the limit $L \rightarrow \infty$. Note that as V_0 is increased, the phenomenon of quasi-trapping appears at smaller L , leading to a shift of the peak emission to the left. The maximum sound emission occurs for large V_0 (and small enough L) since then the density gradient experienced by the soliton is maximised. This trend appears to be maintained with indefinite increase in V_0 , although it requires smaller step widths, which will ultimately become unphysical. When $V_0 > \mu$, the soliton undergoes elastic reflection with no sound emission, provided the step width L is sufficiently long to allow for complete fluid healing to the imposed potential V_0 . This explains the tailing off of the sound energy for $V_0 = 2\mu$ (solid line) to zero as $L > 5\xi$.

Our analysis so far has been based on a soliton of fixed initial speed, and this has enabled us to map the entire dependence of emitted sound energy on L and V_0 for a particular soliton speed. We shall now briefly comment on the dependence of the emitted energy on initial soliton speed. Fig. 4 shows the energy radiated by a soliton incident on a finite potential step of fixed length $L = 5\xi$ and variable height V_0 , for various initial soliton speeds, with the energies scaled in terms of the initial soliton energies. In the regime of transmission over the step (i.e. leftmost part of the figure), the slowest soliton emits the most sound energy. This can be attributed to the fact that, although all three solitons experience the same density gradient, the slowest soliton (solid line) spends the longest time at the step, thereby leading to the greatest time-integrated sound emission. However, the slowest soliton features the deepest density profile. Its passage into the step region is therefore most restricted, causing it to be the first to both reflect and reach the point of saturation of the sound emission (i.e. $V_0 = V_0^m(L)$). Thus, increasing initial soliton speed leads to a general shift of the emission curves to higher potentials. Faster solitons can pass a greater distance into the step region, probing higher density gradients, and so have higher peak sound emission. However, the energy of an unperturbed soliton on a

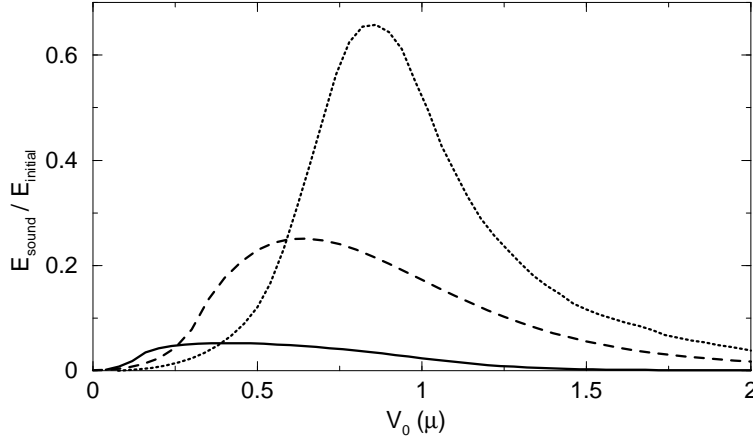


Figure 4. Fraction of the initial soliton energy that is emitted for a soliton incident on a finite potential step of length $L = 5\xi$ as a function of step height V_0 for various initial soliton speeds: $v = 0.3c$ (solid line), $0.5c$ (dashed line - this corresponds to dashed line in Fig. 2(d)), and $0.7c$ (dotted line). The initial soliton energies are 1.157μ , 0.866μ and 0.486μ respectively.

homogeneous background is given by [21],

$$E_{\text{sol}} = \frac{4}{3}\hbar cn \left[1 - \left(\frac{v}{c} \right)^2 \right]^{3/2} \quad (5)$$

and hence, faster solitons have lower energies. This means that, in addition to radiating more energy, faster solitons radiate a higher fraction of their total energy. For example, a soliton with initial speed $v = 0.7c$ can radiate as much as 65% of its initial energy. In all cases the sound emission eventually tends to zero as the step height V_0 becomes much greater than the chemical potential, although faster solitons still emit more energy in the limit of high barriers.

We note that for effectively finite step sizes the soliton undergoes considerable physical deformation as it interacts with the barrier, due to the continuous sound emission. In particular the soliton profile becomes asymmetrically distorted from its equilibrium state, which signifies a deviation of the centre of mass from the density minimum. A detailed quantitative study of the deformation is limited by the rapid change of the soliton profile when it is incident on the barrier. To illustrate these effects more clearly, we therefore turn our attention to linear ramps, for which the soliton, once on the ramp, experiences a constant force.

3. Soliton under uniform acceleration

A linear potential provides a simple way of imparting a controlled and constant force to the soliton. As the soliton ascends the ramp, its depth stays (approximately) constant while the ambient density constantly decreases. At the point where the node of the soliton touches zero density, the soliton reverses direction, and begins to descend the ramp. We observe continuous sound emission from the soliton while it is on the ramp. This causes small deviations from the corresponding classical trajectory, as shown in Fig. 5.

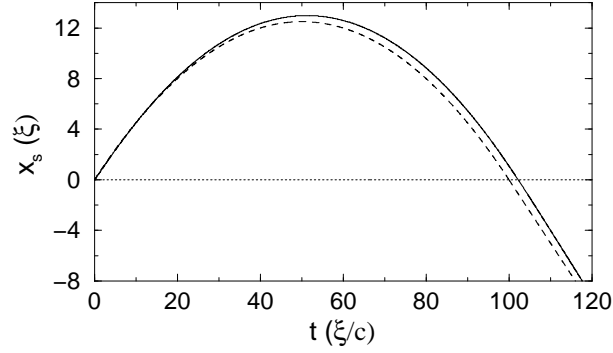


Figure 5. Path of a soliton (solid line), with initial speed $v = 0.5c$, ascending and subsequently descending a linear potential ramp $V = 2 \times 10^{-2}x$ acting in the $x > 0$ region. Due to the sound emission this trajectory deviates from the constant mass effective particle prediction (dashed line).

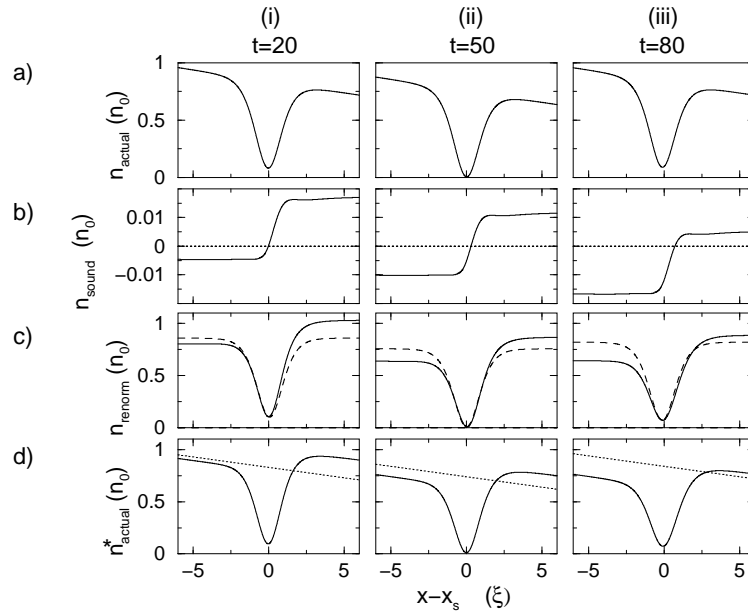


Figure 6. a) Actual density profile of the soliton region, for the case of propagation on a linear ramp with the same parameters as Fig. 5, during (i) ascent ($t = 20\xi/c$), (ii) the turning point ($t = 50\xi/c$), and (iii) descent ($t = 80\xi/c$). b) Sound density within the soliton region, obtained as follows: Firstly, we subtract the background density from the actual soliton profile, to obtain a ‘renormalised’ soliton profile. Then, by subtracting from this the corresponding *unperturbed* soliton with the same speed and position (dashed line in (c)), we isolate the sound density. The renormalised soliton profile, with the sound density (b) magnified by a factor of ten, is shown by the solid line in (c), and clearly illustrates the sound-induced deformation. d) Same as (a) but, again, with the sound density magnified by a factor of ten (solid line). The dotted line indicates the corresponding time-independent background density.

Shapshots of the perturbed soliton and the corresponding sound density, for a soliton (i) ascending up the ramp, (ii) at the stationary point, and (iii) during descent are shown in Fig. 6. The sound density (Fig. 6(b)) consists of a higher density in front of the soliton and a lower density behind it, the fore and aft pulses being spatially compressed and extended depending on the relative motion of the soliton and sound through the fluid. Note that, at the stationary point, where there is no relative motion between soliton and sound field, the fore and aft density pulses have equal (but opposite) amplitudes. The asymmetrically emitted sound within the soliton region leads to an apparent deformation of the soliton profile. This deformation can be visualised by comparing the renormalised soliton (i.e. soliton profile minus background density) to a corresponding unperturbed soliton of the same speed and position (Fig. 6(c)). This deformation leads to a shift of the soliton centre of mass \bar{x} from the density minimum x_s [44], where the soliton centre of mass is defined as

$$\bar{x} = \frac{\int_s x (|\psi|^2 - n) dx}{\int_s (|\psi|^2 - n) dx}. \quad (6)$$

and the ‘soliton region’ S is taken to be $(x_s \pm 5\xi)$. For a soliton on a ramp, this yields a constant shift of the centre of mass from the soliton density minimum [45], indicating a link between soliton deformation and acceleration.

The exception to this link arises when the whole fluid itself is accelerated. The fluid motion then also accelerates the soliton, from the viewpoint of a stationary observer, but the soliton is not accelerated with respect to the background fluid. This could be achieved, for example, by displacing the confining potential such that the whole system (background fluid plus soliton) move together. Such motion does not induce a deformation of the soliton profile and therefore does not lead to sound emission. From now on, when referring to acceleration we therefore mean acceleration with respect to the background fluid.

The power radiated by the soliton while on a ramp is shown in Fig. 7(a), as a function of the deformation parameter $(\bar{x} - x_s)$, for various initial soliton speeds. This suggests a behaviour of the form

$$\frac{dE_s}{dt} = -\kappa(\bar{x} - x_s)^\alpha \quad (7)$$

where the value of κ is expected to depend, at least, on the initial soliton speed and the gradient of the local density. Fig. 7(b) plots the same information on a logarithmic scale, thereby confirming the above behaviour. From this we determine, to very good approximation, the value $\alpha = 2$. Fig. 7(c) shows, on logarithmic scale, the relation between the deformation parameter and the soliton acceleration, for the case of a soliton ascending a ramp. This points to a direct proportionality between the two quantities, which is consistent with an acceleration-squared law for emitted power [19, 22].

4. Soliton oscillating in a gaussian trap

The relation between emitted power and soliton deformation can be put on firmer ground by considering the case of an oscillating soliton, since such a case includes a wide range of soliton speeds and background densities. The most lucid example is that of a symmetrical trap formed by two gaussian-shaped potentials,

$$V = V_0 \left[\exp \left\{ -\frac{(x - x_0)^2}{w^2} \right\} + \exp \left\{ -\frac{(x + x_0)^2}{w^2} \right\} \right], \quad (8)$$

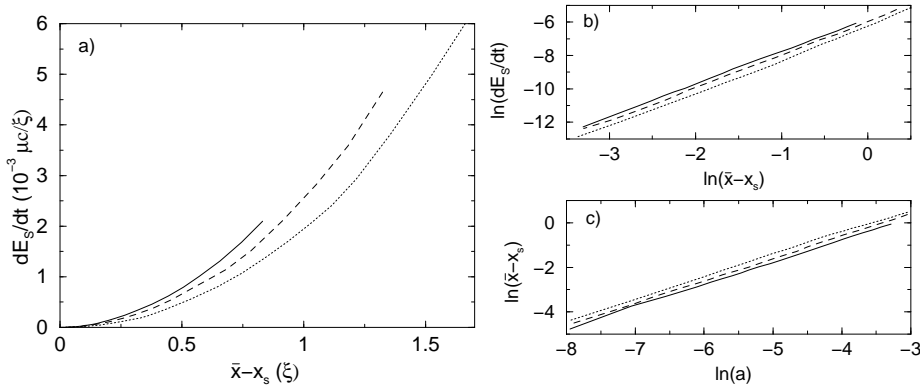


Figure 7. a) Power radiated from a soliton ascending, and subsequently descending, a linear ramp, plotted versus the soliton deformation $(\bar{x} - x_s)$. Different curves correspond to different initial soliton speeds $v = 0.3c$ (solid line), $0.5c$ (dashed line) and $0.7c$ (dotted line). Each curve has been constructed by probing over different potential gradients, in the range $(10^{-3} - 10^{-1})\mu/\xi$. Note that solitons with larger initial speeds ascend higher up the ramp and the maximum observable deformation increases with increasing initial soliton speed. b) Same data plotted on log-log scale. c) Soliton deformation versus acceleration (measured in units of (c^2/ξ)) on log-log scale, for the above mentioned soliton ascending a linear ramp.

within which the soliton is initially trapped, as illustrated in Fig. 8. Here V_0 is the amplitude of the gaussians, x_0 the distance of the centres from the origin, and w the gaussian width. To monitor the effect of sound emission (without allowing for reabsorption of sound to complicate matters [19]) we assume that the height of the gaussian bump is low enough ($V_0 \ll \mu$), such that the emitted sound escapes the system. To avoid reabsorption of sound, one would need to embed this double gaussian trap in a weaker (harmonic) outer trap. Then, as the soliton oscillates in the (inner) double gaussian trap, it emits counter-propagating sound waves which, for sufficiently low V_0 , ‘escape’ to the outer trap and do not re-interact with the soliton (within the timescales of interest). This results in a drastic change in the soliton amplitude and frequency.

In the last section we argued that the deformation of the soliton is intimately linked with the continuous sound emission, and gave evidence to suggest that the power emitted by the soliton can be parametrised by the square of the soliton deformation. However, the coefficient κ in Eq. (7) will *not*, in general, be a constant depending *simply* on *initial* soliton speed, due to the changing background density gradient in the trap. We therefore anticipate κ to depend on the position of the soliton in the trap (and hence become a function of the local background speed and density) in a non-trivial manner.

Fig. 9 considers the long term dynamics of a soliton with initial speed $0.3c$ oscillating in a double gaussian trap. The radiation from the oscillating soliton leads to an ‘anti-damping’ effect [26], whereby the soliton oscillates progressively faster and with greater amplitude (see Fig. 9(a) for $t < 4000\xi/c$). This leads to an initial *decrease* in the oscillation period (Fig. 9(b)) [31], and a significant deviation from the corresponding energy-conserving trajectory (dashed line in Fig. 9(a)). However, as

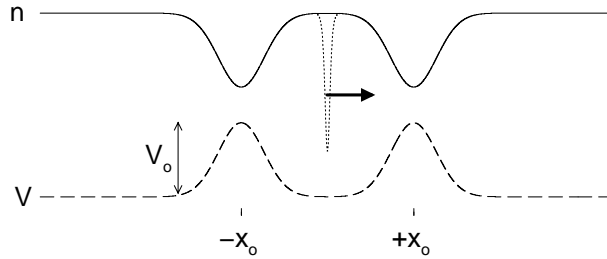


Figure 8. A dark soliton (dotted line) is confined to oscillate within a trap formed by two identical gaussian bumps (dashed line) of height V_0 centred at $-x_0$ and $+x_0$. The solid line represents the corresponding time-independent background density.

the soliton begins to probe the outer regions of the trap, where the potential gradient tails off, the period *increases*. Eventually, at $t \approx 6500$ the soliton has lost sufficient energy to escape the trap [19, 26, 27].

The periodic deformation of the soliton as it oscillates in the trap is shown in Fig. 9(c). The deformation is clearly zero when the soliton passes through the minimum of the trap, where the background density is effectively homogeneous, and becomes maximum at the extremum of each oscillation. The energy of the soliton (Fig. 9(d)) decreases in periodic steps, due to the periodic sound emission shown in Fig. 9(e), with both of these (shown by solid lines) determined numerically from Eq. (4). The peak periodic values of both sound emission rate (Fig. 9(e)) and soliton deformation (Fig. 9(c)) initially increase in time as the soliton probes further and further into the double gaussian trap, where the background density gradient becomes *higher*. Later in the evolution, the peaks begin to decrease in amplitude and develop intermediate dips as the soliton probes the outer, essentially harmonic regions of the trap where the potential tails off and the density gradient *decreases*. Also plotted in Fig. 9(e) is the power emission predicted by Eq. (7) (dotted line) with $\alpha = 2$ and a suitably chosen value of κ , such that the initial peak emission rates match. The agreement is found to be very good, particularly at early times, when the soliton is localised within the central region of the trap. However, the non-uniformly increasing background density gradient in the trap under consideration causes a degraded agreement at later times. We attribute this to the deviation of the coefficient κ in Eq. (7) from the effectively constant value assumed here.

To investigate the validity of Eq. (7) in more detail, we next investigate the two ‘limiting’ regimes of soliton motion arising in Fig. 9. These correspond to (i) the case of a soliton oscillating near the centre of the double gaussian trap (for which the density gradient increases monotonically as one moves away from the trap centre, roughly $t < 2000(\xi/c)$ in Fig. 9), and (ii) the limit of a soliton oscillating essentially all the way to the edges of the trap, and thus probing both the initial monotonic increase of the background density to its maximum value, and its subsequent decrease (corresponding roughly to $t > 4000(\xi/c)$ in Fig. 9). To look into these effects more clearly, we investigate respectively the cases of a slower and a faster soliton, compared to the initial soliton speed of Fig. 9. This will also display more clearly the two competing mechanisms contributing to the change in the soliton oscillation frequency evident in Fig. 9(a).

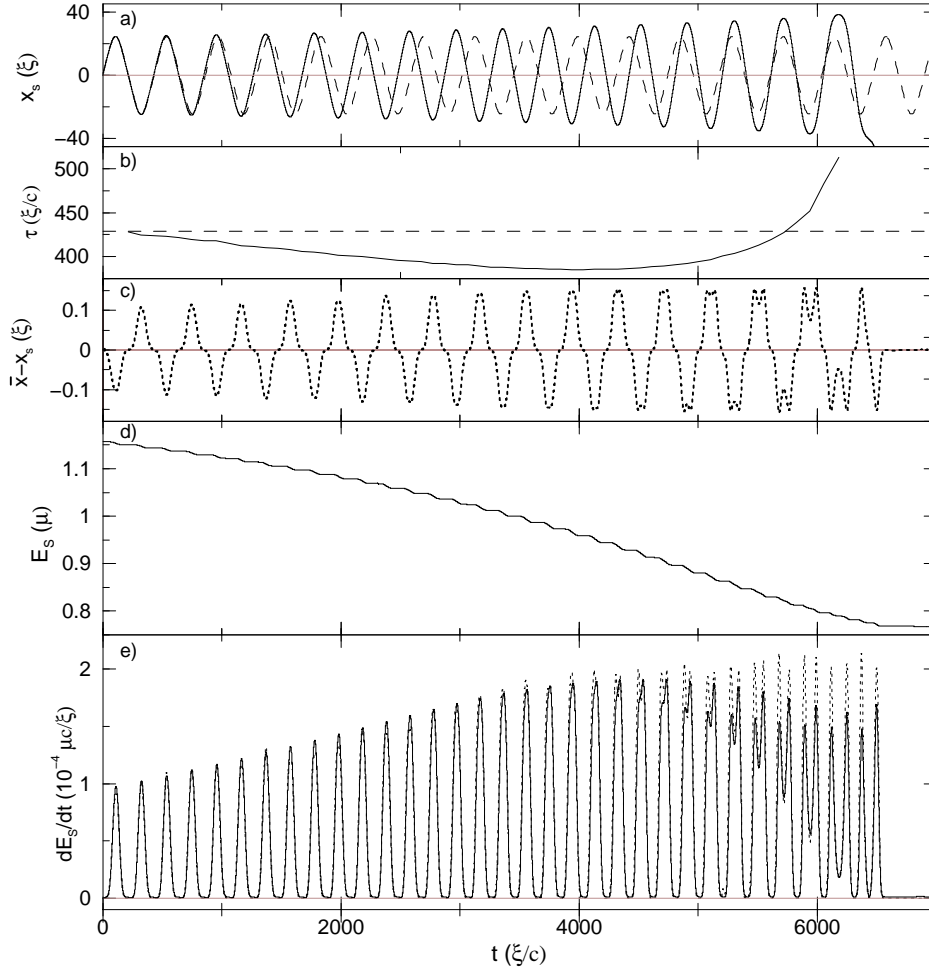


Figure 9. a) Path of a dark soliton (solid line) with initial speed $0.3c$ oscillating in the double gaussian trap of Eq. (8) with $V_0 = 0.3\mu$, $x_0 = 40\xi$, and $w^2 = 200\xi^2$, along with the corresponding non-dissipative trajectory (dashed line). The low amplitude chosen ($V_0 = 0.3\mu$) ensures that the radiation escapes the inner region. b) Oscillation period of the soliton τ (solid line) and effective particle of constant mass (dashed line) as a function of time c) Deformation parameter of the soliton ($\bar{x} - x_s$) versus time d) Decay of soliton energy as a function of time. e) Power emitted by the soliton as a function of time computed from the energy functional Eq. (4) (solid line) versus the prediction of Eq. (7) with $\alpha = 2$ and $\kappa = 0.0107(\mu c/\xi^3)$ (dotted line).

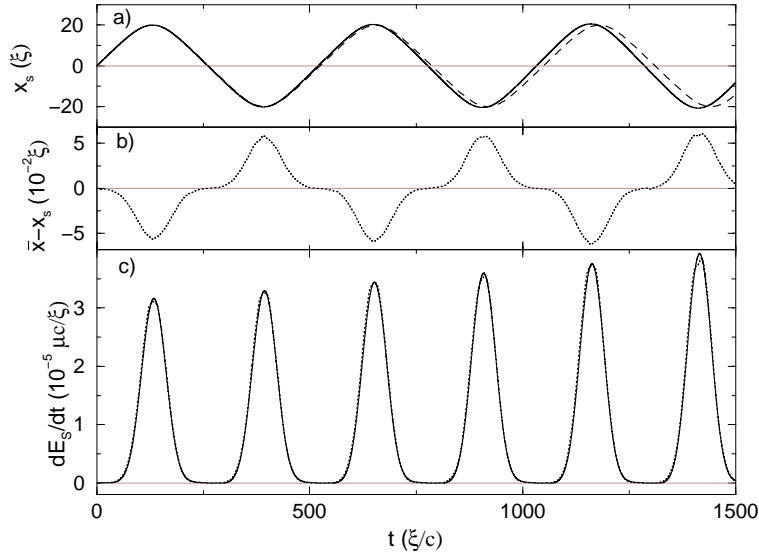


Figure 10. a) Path of a dark soliton (solid line) and the corresponding non-dissipative particle (dashed line), with initial speed $0.2c$, oscillating in the same trap of Fig. 9. b) Deformation parameter of the soliton ($\bar{x} - x_s$) as a function of time. c) Power emitted by the soliton as a function of time, as computed from the energy functional Eq. (4) (solid line), versus the deformation squared prediction of Eq. (7) with $\alpha = 2$ and $\kappa = 0.0107(\mu c/\xi^3)$ (dotted line).

Fig. 10 considers a soliton with slow initial speed, $v = 0.2c$, oscillating in a double gaussian trap with the same parameters as in Fig. 9. In particular, Fig. 10(a) shows the deviation of the soliton oscillations from the corresponding non-dissipative predictions, with the soliton oscillating faster than the non-dissipative case, as a result of sound emission. The resulting soliton deformation is illustrated in Fig. 10(b). Finally, Fig. 10(c) compares the measured energy loss from Eq. (4) (solid line) to the prediction of Eq. (7) (dotted line), yielding remarkable agreement.

The opposite regime of a sufficiently fast soliton probing the entire structure of the double gaussian trap is shown in Fig. 11. In this regime, the soliton experiences more complicated dynamics due to the tailing off of the gaussian potential. Firstly we see that, contrary to the case of a slow soliton (Fig. 10(a)), the fast soliton (Fig. 11(a)) oscillates *slower* than the corresponding non-dissipative trajectory. Furthermore, the deformation parameter ($\bar{x} - x_s$) plotted in Fig. 11(b) now develops intermediate dips at the extrema of each oscillation. Both of these effects are due to the nature of the changing background density in the double gaussian trap. Although this gradient initially increases with increasing deviation from the trap centre, it subsequently reaches a maximum and then starts decreasing again, such that the soliton period increases drastically as it spends more and more time at the edges of the trap. This also explains the intermediate dips in the rate of sound emission shown in Fig. 11(c). Fig. 11(b) further compares the deformation parameter to the local soliton acceleration computed numerically. This yields an exact proportionality, confirming our earlier claim of Sec. 3. Fig. 11(c) compares the rate of sound emission in time as computed from Eq. (4) (solid line), to the prediction of Eq. (7) based on a *constant* coefficient

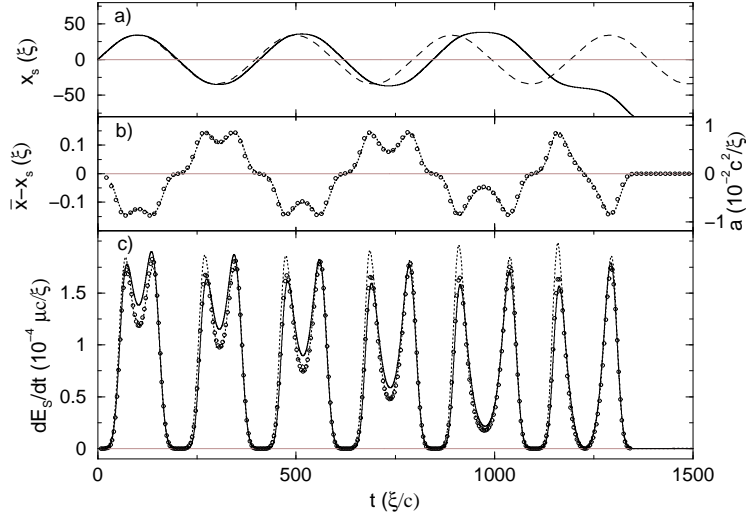


Figure 11. a) Path of a dark soliton (solid line) with initial speed $0.5c$, and the corresponding non-dissipative particle (dashed line), oscillating in the same double gaussian trap as in Fig. 9. b) Deformation parameter of the soliton ($\bar{x} - x_s$) (dotted line) (left axis), and soliton acceleration (open circles) (right axis) versus time. c) Power emitted by the soliton as a function of time computed from the energy functional (Eq. (4)) (solid line), versus the deformation squared prediction of Eq. (7) with $\alpha = 2$ and $\kappa = 0.0107(\mu c/\xi^3)$ (dotted line). Also shown is the acceleration squared power emission predicted by Eq. (9) (open circles).

κ (dotted line). Although the intermediate dip is correctly accounted for by Eq. (7), the incorrect assumption of a constant κ leads to a slight overestimate of the peak energy emission, with the discrepancy increasing as the soliton probes the very edge of the trap. These two results are further compared to an analytical prediction for sound emission from an unstable dark soliton (on a *homogeneous* background) derived within the context of nonlinear optics [22]. The applicability of this theory to inhomogeneous systems has been discussed in [19]. This theory predicts that the breakdown of integrability of the cubic NLSE leads to a rate of energy loss

$$\frac{dE_s}{dt} = -L_s(v, n) \left(\frac{dv}{dt} \right)^2, \quad (9)$$

where

$$L_s(v, n) = \frac{c}{c^2 - v^2} \left[\frac{2c^2}{n} \left(\frac{\partial N_s}{\partial v} \right)^2 + 2v \left(\frac{\partial N_s}{\partial v} \right) \left(\frac{\partial S_s}{\partial v} \right) + \frac{n}{2} \left(\frac{\partial S_s}{\partial v} \right)^2 \right]. \quad (10)$$

Here n is the local background density, S_s the total phase slip across the moving soliton, and $N_s = \int (n - |\psi|^2) dz$ is the number of particles displaced by the soliton.

The prediction of Eqs. (9)-(10) shown by the open circles in Fig. 11(c) indeed yields near perfect agreement with the energy functional calculations of Eq. (4). The peaks in power emission are now correctly accounted for, due to the constantly

adjusting proportionality coefficient $L_s(v, n)$ of Eq. (9). Since Fig. 11(b) proves an exact proportionality between acceleration and deformation parameter, we conclude that the inadequacy of Eq. (7) in the limit of solitons probing the edge of the trap is due to the oversimplified assumption of a constant coefficient of proportionality κ . Assigning a slightly varying κ which depends on the local n and v in a manner similar to the dependence of L_s on these parameters will clearly remedy this apparent inaccuracy of Eq. (7). Nonetheless, it is remarkable that even the oversimplified assumption of a *constant* κ yields reasonable values for the rate of sound emission.

5. Discussion

We have examined soliton dynamics and sound emission due to various forms of background density perturbations in one dimension and have quantified the sound emission in terms of the step geometry. We have shown that a dark soliton incident upon a potential step can emit a significant fraction of its energy. For example, a soliton with initial speed $v = 0.7c$ can emit *more than 60% of its energy* in its interaction with the step.

By considering smoother density inhomogeneities, we have shown that the gradient of the background density results in a deformation of the soliton profile, in the sense that the soliton centre of mass on an inhomogeneous background deviates from the soliton density minimum. The reason for this ‘mismatch’ is clear: As the soliton propagates through the inhomogeneous region, it is induced to emit counter-propagating waves (with positive and negative amplitudes with respect to the background density), each of which moves with the local speed of sound. However, the *relative* motion of the emitted sound waves to the soliton minimum depends on the direction of motion of the soliton. This means that the sound wave moving in the soliton direction with speed $(c - v)$ is more compressed than the one moving in the opposite direction at speed $(c + v)$. We note that, strictly speaking, one cannot distinguish between soliton and sound energy trapped within the soliton region, and this would also be true for any experimental measurement of the soliton profile. Hence, the soliton profile essentially includes the amount of emitted sound which has not yet escaped the soliton region and this leads to the apparent deformation of the soliton. This deformation was shown to be directly proportional to the acceleration of the soliton through the fluid (determined as the acceleration of the density minimum). More importantly we have shown that the energy emitted by the soliton due to background inhomogeneities can be parametrised in terms of the square of both this deformation parameter and, hence, of the acceleration. The coefficient of proportionality is, to reasonable approximation constant, depending on initial soliton speed and background density gradient. However, a more accurate determination would require the calculation of its value at each position, since, in general, it will depend on the *local* soliton speed and background density.

Acknowledgments

We acknowledge financial support from the UK EPSRC.

References

- [1] L. Deng, E. W. Hagley, J. Wen, M. Trippenbach, Y. Band, P. S. Julienne, J. E. Simsarian, K. Helmerson, S. L. Rolston, and W. D. Phillips *Nature* **398**, 218-220 (1999).
- [2] K. E. Strecker, G. B. Partridge, A. G. Truscot, and R. G. Hulet, *Nature* **417**, 150 (2002).
- [3] L. Khaykovich, F. Schreck, G. Ferrari, T. Bourdel, J. Cubizolles, L. D. Carr, Y. Castin, and C. Salomon, *Science* **296**, 1290 (2002).
- [4] J. Denschlag, J. E. Simsarian, D. L. Feder, C. W. Clark, L. A. Collins, J. Cubizolles, L. Deng, E. W. Hagley, K. Helmerson, W. P. Reinhardt, S. L. Rolston, B. I. Schneider, and W. D. Phillips, *Science* **287**, 97 (2000).
- [5] S. Burger, K. Bongs, W. Ertmer, K. Sengstock, A. Sanpera, G. V. Shlyapnikov, and M. Lewenstein, *Phys. Rev. Lett.* **83**, 5198 (1999).
- [6] Z. Dutton, M. Budde, C. Slowe, and L. V. Hau, *Science* **293**, 663 (2001).
- [7] Y. S. Kivshar and D. E. Pelinovsky, *Phys. Rep.* **331**, 117 (2000).
- [8] G. P. Agrawal, *Nonlinear Fiber Optics*, 2nd edition (Academic Press, 1995).
- [9] P. D. Miller, *Phys. Rev. E* **53**, 4137 (1996).
- [10] A. Gorlitz, J. M. Vogels, A. E. Leanhardt, C. Raman, T. L. Gustavson, J. R. Abo-Shaeer, A. P. Chikkatur, S. Gupta, S. Inouye, T. Rosenband, and W. Ketterle, *Phys. Rev. Lett.* **87**, 130402 (2001).
- [11] F. Schreck, L. Khaykovich, K. L. Corwin, G. Ferrari, T. Bourdel, J. Cubizolles, and C. Salomon, *Phys. Rev. Lett.* **87**, 080403 (2001).
- [12] W. Hansel, P. Hommelhoff, T. W. Hansch, and J. Reichel, *Nature* **413**, 498 (2001).
- [13] H. Ott, J. Fortagh, G. Schlotterbeck, A. Grossmann, and C. Zimmermann, *Phys. Rev. Lett.* **87**, 230401 (2001).
- [14] S. Schneider, A. Kasper, C. vom Hagen, M. Bartenstein, B. Engeser, T. Schumm, I. Bar-Joseph, R. Folman, L. Feenstra, and J. Schmiedmayer, *Phys. Rev. A* **67**, 023612 (2003).
- [15] A. D. Jackson, G. M. Kavoulakis, and C. J. Pethick, *Phys. Rev. A* **58**, 2417 (1998).
- [16] A. E. Muryshev, H. B. van Linden van den Heuvell, and G. V. Shlyapnikov, *Phys. Rev. A* **60**, R2665 (1999).
- [17] A. Muryshev, G. V. Shlyapnikov, W. Ertmer, K. Sengstock, and M. Lewenstein, *Phys. Rev. Lett.* **89**, 110401 (2002).
- [18] G. Huang, J. Szeftel, and S. Zhu, *Phys. Rev. Lett.* **65**, 053605 (2002).
- [19] N. G. Parker, N. P. Proukakis, M. Leadbeater, and C. S. Adams, *Phys. Rev. Lett.* accepted, cond-mat/0212278.
- [20] V. E. Zakharov and A. B. Shabat, *Sov. Phys. JETP* **34**, 823 (1973).
- [21] Y. S. Kivshar and B. Luther-Davies, *Phys. Rep.* **278**, 81-197 (1998).
- [22] D. E. Pelinovsky, Y. S. Kivshar, and V. V. Afanasjev, *Phys. Rev. E* **54**, 2015 (1996).
- [23] D. L. Feder, M. S. Pindzola, L. A. Collins, B. I. Schneider, and C. W. Clark, *Phys. Rev. A* **62**, 053606 (2000).
- [24] J. Brand and W. P. Reinhardt, *Phys. Rev. A* **65**, 043612 (2002).
- [25] S. Komineas and N. Papanicolaou, *Phys. Rev. A* **67**, 023615 (2003).
- [26] T. Busch and J. R. Anglin, *Phys. Rev. Lett.* **84**, 2298 (1999).
- [27] P. O. Fedichev, A. E. Muryshev, and G. V. Shlyapnikov, *Phys. Rev. A* **60**, 3220 (1999).
- [28] M. A. de Moura, *J. Phys. A* **27**, 7157 (1994); M. A. de Moura, *Phys. Rev. A* **37**, 4998 (1988).
- [29] S. A. Morgan, R. J. Ballagh, and K. Burnett, *Phys. Rev. A* **55**, 4338 (1997).
- [30] W. P. Reinhardt and C. W. Clark, *J. Phys. B* **30**, L785 (1997).
- [31] V. A. Brazhnyi, A. M. Kamchatnov, and V. V. Konotop, preprint cond-mat/0301319.
- [32] Y. S. Kivshar and X. Yang, *Phys. Rev. E* **49**, 1657 (1994).
- [33] V. V. Konotop and V. E. Vekslerchik, *Phys. Rev. E* **49**, 2397 (1994).
- [34] A. B. Aceves, J. V. Moloney, and A. C. Newell, *Phys. Rev. A* **39**, 1809 (1989).
- [35] Y. S. Kivshar, A. M. Kosevich, and O. A. Chubykalo, *Phys. Rev. A* **41**, 1677 (1990).
- [36] Y. S. Kivshar and M. L. Quiroga-Teixeiro, *Phys. Rev. A* **48**, 4750 (1993).
- [37] G. Huang, M. G. Velarde, and V. A. Makarov, *Phys. Rev. A* **64**, 013617 (2001).
- [38] D. J. Frantzeskakis, G. Theocharis, F. K. Diakonov, P. Schmelcher, and Y. S. Kivshar, *Phys. Rev. A* **66**, 053608 (2002).
- [39] H.E. Nistazakis, D. J. Frantzeskakis, N. Brouzakis, F. K. Diakonov, P. Schmelcher, and J. Schmiedmayer, preprint cond-mat/0211702.
- [40] V. V. Konotop, V. M. Perez-Garcia, Y. F. Tang, and L. Vazquez, *Phys. Lett. A* **236**, 314 (1997).
- [41] L. D. Carr, J. Brand, S. Burger, and A. Sanpera, *Phys. Rev. A* **63**, 051601 (2001).
- [42] L. D. Carr, C. W. Clark, and W. P. Reinhardt, *Phys. Rev. A* **62**, 063610 (2000).
- [43] L. D. Carr, K. W. Mahmud, and W. P. Reinhardt, *Phys. Rev. A* **64**, 033603 (2001).

- [44] For a harmonic trap, soliton deformation has also been found in [31].
- [45] A soliton on a ramp experiences a constant acceleration, and one can thus transform to the accelerating frame via the transformations $x \rightarrow x - 2\alpha t^2$ and $\psi \rightarrow \exp(2i\alpha x t + 4i\alpha^2 t^3/3)\psi$ (H. H. Chen and C. S. Liu, Phys. Rev. Lett. **37**, 693 (1976)). The usual dark soliton expression of Eq. (2) will hold then, with all quantities referring to the corresponding values in the *accelerating* frame.